Current Research in Biotechnology 7 (2024) 100189

Contents lists available at ScienceDirect

Current Research in Biotechnology

journal homepage: www.elsevier.com/locate/crbiot

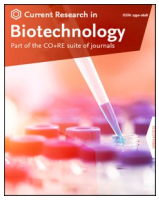

Production of genetically engineered designer biodiesel from yeast lipids

Benjamin Ouellet, A.M. Abdel-Mawgoud *

Department of Biochemistry, Microbiology and Bioinformatics, Faculty of Science and Engineering, Laval University, 1045 Ave. de la Médecine, Quebec, QC G1V 0A6, Canada
Institute of Integrative Biology and Systems, Laval University, 1030 Ave. de la Médecine, Quebec, QC G1V 0A6, Canada

ARTICLE INFO

Keywords:
Oleaginous yeasts
Rhodotorula toruloides
Lipomyces starkeyi
Starmerella bombicola
Yarrowia lipolytica
Mathematical modeling
Full factorial design of experiments
Biofuel
Genetically engineered biodiesel

ABSTRACT

Biodiesels constitute a growing class of fuel in a world that is increasingly inclined towards more ecological and sustainable energy. Despite their many advantages, biodiesels have limited cold flow properties and larger NO_X emissions. These limitations are mostly attributed to the chemical compositions of biodiesels which are dictated by the chemical compositions of their feedstock oils. Accordingly, this study presents a novel approach to produce Genetically Engineered Biodiesel (GEB) whose chemical composition can be controlled by the genetic manipulation of oleaginous yeast oils for the production of designer biodiesels with improved properties and performances. Using full-factorial central composite design, the best chemical composition of an optimal biodiesel was predicted. Then, simple and combined *MFE1*, *PEX10* and *POX2* mutants of the oleaginous yeast *Yarrowia lipolytica* were constructed. These mutants showed interesting lipid profiles where their biodiesels are predicted to have better cold flow properties. These mutants showed also higher lipid titers by 2–3 folds compared to the parent strain. This study provides an approach for tailor designing of biodiesel properties and performances via genetic engineering. Moreover, it provides solutions potentially enabling biodiesel to be used as a standalone fuel in cold climates without any mixing with petrodiesel.

1. Introduction

The worldwide interest in developing sustainable and renewable fuels is growing in view of the environmental concerns and depleting global reserves of fossil fuels. In such a context, biodiesels are placed at the center of attention as one of the best alternatives. Biodiesels are fatty acid methyl esters (FAME) produced by the methyl transesterification (methanolysis) of triacylglycerols of biological oils. Compared to petrodiesels, biodiesels have the advantage of generating lesser emissions of CO, SO_2, unburnt hydrocarbons (UHC) and particulate matters (PM) while having higher cetane numbers (CN). CN is a metric of the combustion speed or autoignition-upon-compression performance in compression ignition (CI) engines; the higher the CN the higher is the speed of ignition and combustion (Ramirez-Verduzco et al., 2012). However, biodiesels have some drawbacks relative to petrodiesel where biodiesels have lower heating value, higher viscosity and higher NO_X emissions (Hoekman et al., 2012; Pinzi et al., 2013) together with poorer properties and performances at low-temperatures (Park et al., 2008; Su et al., 2011). The cold flow properties are described by the Cloud Point (CP), Pour Point (PP) and Cold Filter Plugging Point (CFPP) that are respectively referring to the temperature at which the fuel jellifies, the lowest temperature where fuel is able to flow in the engine and the temperature at which fuel clogs the filter (Dunn, 2015). The poor cold flow properties are concerning particulalry in colder environments where biodiesel can clog the fuel line, filter, and engine fuel injector, hence limiting its operability (Wahlen et al., 2013; Wu et al., 2009). Consequently, biodiesels have to be blended with petrodiesel mostly as B5 (5 % biodiesel, 95 % diesel) or less frequently as B20 to profit from the reduced emission properties of biodiesel while profiting from the good operability of diesel (Joshi and Pegg, 2007).

The properties and performances of both diesel and biodiesel are implied by their chemical composition (Hoekman et al., 2012). Being esters of fatty acids, biodiesel have higher oxygen content than diesel that leads to more complete fuel combustion and hence lesser CO, PM, and UHC emissions, yet higher NO_X emissions and viscosity (Hoekman et al., 2012; Pinzi et al., 2013). The higher NO_X emissions of biodiesel is probably due to the reaction of oxygen atoms of FAMEs with air nitrogen during combustion. FAMEs also differ from diesel in having a higher carbon content and unsaturation degree that correlates with improved combustion and physical properties, yet worse emission profiles

* Corresponding author at: Pavillon Charles-Eugène-Marchand, 1030, avenue de la Médecine, Room 3167 (Office), Québec, Québec G1V 0A6, Canada.
E-mail address: ahmad.saleh@bcm.ulaval.ca (A.M. Abdel-Mawgoud).

https://doi.org/10.1016/j.crbiot.2024.100189
Received 7 October 2023; Received in revised form 12 January 2024; Accepted 8 February 2024
Available online 14 February 2024

(Hoekman et al., 2012; Pinzi et al., 2013) (Table 3).

Biodiesel has gone through several developmental generations aiming at producing it in less costly and more ethical manner (Singh et al., 2020). First generation biodiesel, which constitutes the largest share in the current biodiesel industry, relies on edible vegetable oil (e.g. rapeseed, palm and soybean oils) and thus is raising ethical concerns for its occupation of cultivable lands and for its consumption of edible oils as feedstocks for fuel production rather than feeding human. These concerns are partly resolved in second-generation biodiesel that relies on non-edible feedstock instead (e.g. jatropha oil and waste oils), although this generation has limited feedstock alternatives and is associated with high production cost (Singh et al., 2020). The third generation biodiesel originates mainly from marine organisms, e.g. from microalgal biomass, that comes with the advantage of being able to use CO_2 as the carbon source (Singh et al., 2020). Fourth generation biodiesel uses microbial single-cell and microalgal oils as feedstocks, and also employs genetic engineering of single-cell biomass to enhance the photoconversion efficiency of CO_2 and light as carbon and energy sources into biofuel. Although the microalgal biodiesel has the potential for developing a sustainable circular bioeconomy by absorbing the cheaply available atmospheric carbon, CO_2, thus reducing both cost of production and green house gases, microalgal biodiesel are highly polyunsaturated (Hoekman et al., 2012) which has a negative impact on its oxidative stability and combustion properties (Knothe, 2008). Moreover, microalgae grow slowly and require peculiar photobioreactor designs with large illuminated surfaces and mechanisms to prevent biofilm formation (Okoro et al., 2019). Although open cultivation of microalgae is an alternative, yet it depends on sun light which is however limited in certain countries.

Microbial oils from yeast and bacteria are better alternatives to microalgal oils for many reasons. Oleaginous yeasts for example can achieve lipid contents of up to 70 % compared to 25 % in oleaginous microalgae (Zhang et al., 2021) in regular bioreactors (Okoro et al., 2019). Interestingly, apart from some variation in the unsaturation degree, yeast oils have similar properties to soybean oil that is currently the main feedstock used for biodiesel production (Wahlen et al., 2013).

The properties and performances of biodiesel are dictated by its chemical composition which stems from the chemical composition of used feedstock oils. Based on this fact, the term "designer biodiesel" emerged (Knothe, 2008; Anuchaya et al., 2016) that involves the modulation of the FAME composition of biodiesel to improve their properties and performances while meeting the international American (ASTM, 2023) and European (En, 2019) standard biodiesel specifications (Table 4). Current strategies for modulation of biodiesel chemistry in "Designer biodiesel" involve modulations upstream, midstream or downstream to the transesterification process. Modulation upstream to transesterification involves the careful blending of vegetable oils from different sources and compositions in specific ratios to achieve a desired overall chemical composition before transesterification of the oil blend into biodiesel (Knothe, 2008; Anuchaya et al., 2016; Kinney and Clemente, 2005). Kinney and Clemente (2005) suggested that genetic modification of the lipid profiles of plant oils, specifically soybean oil, would more efficiently optimize biodiesel properties with respect to oxidative stability and cold flow properties. Modulation midstream to transesterification involves the use of alcohols other than methanol (Knothe, 2008; Knothe, 2005). Using isobutanol or ethanol instead of methanol improves cold flow properties and the heating value of resulting biodiesels, yet at the expense of a greater viscosity and higher cost of production (Knothe, 2008; Knothe, 2005). Modulation downstream to transesterification involves the physical fractionation of heavy biodiesel through winterization (Vijayan et al., 2018), which involves cooling the biodiesel and removing the undesirable heavy biodiesel turned into wax (Knothe, 2008; Vijayan et al., 2018). This winterization results in biodiesels with high unsaturated content and improved cold flow properties at the expense of low biodiesel production yields, low oxidative stability, and greater production cost (Knothe, 2008; Vijayan et al., 2018). Another modulation strategy also downstream to transesterification involves the use of additives (Sorate and Bhale, 2015) that improve oxidative stability or properties at low temperatures, yet their efficiencies are variable depending on biodiesel composition (Sorate and Bhale, 2015).

In this study, a novel strategy is proposed, upstream to transesterification, where the chemical composition of microbial single cell oil is genetically modulated to generate tailored feedstocks for the production of what is named in this study as genetically engineered "designer biodiesel" (GEB). For this goal, the oleaginous yeast *Yarrowia lipolytica* was selected for its abilities to accumulate as much as 70 % of its dry cell weight (DCW) (Beopoulos et al., 2008; Blazeck et al., 2014; Dulermo and Nicaud, 2011; Abdel-Mawgoud et al., 2018), to grow fast on different and cheap carbon sources (Zhao et al., 2015), and for the availability of efficient genome editing protocols for this yeast (Abdel-Mawgoud and Stephanopoulos, 2020; Ouellet and Abdel-Mawgoud, 2023; Schwartz et al., 2016). Moreover, different culture media have been developed to improve lipid yields in *Y. lipolytica* (Ouellet et al., 2023) and different target genes modulating lipogenesis have been identified in this yeast (Wang et al., 2020) that showed to affect the yield and/or the chemical composition of lipids.

To define the benchmark of such genetic engineering of cells as sources of feedstock oils for production of designer biodiesel, a Design of Experiments (DOE) was applied using regression models that were restrained to the limits set by the ASTM and EN biodiesels specifications. The optimal chemical composition supporting optimal biodiesel properties and performance (e.g. cetane number, viscosity and density leading to improved cold flow properties) was predicted as a function of average carbon chain length and unsaturation degree. Using these models, the lipid profile of *Y. lipolytica* PO1f was found out to be very close to the predicted optimum, hence a promising feedstock for the production of biodiesels with optimal properties and performances. Nonetheless, it is predicted to result in a biodiesel with poor cold-flow properties; improving of which was thus the focus of this study.

Mutations of *MFE1*, a multifunctional enzyme responsible for the second and third step of fatty acid β-oxidation, and *PEX10*, peroxisome biogenesis factor, were reported to greatly enhance lipid titers (Blazeck et al., 2014; Dulermo and Nicaud, 2011). Single or combined mutations of the six peroxisome acyl-CoA oxidase homologues (*POX1-6*) in *Y. lipolytica* showed to influence the lipid profile (Mlíčková et al., 2004) as well as to enhance lipid accumulation (Dulermo and Nicaud, 2011). Interestingly, each peroxisome oxidase, *POX1-6*, has a preferred affinity to different chain lengths of fatty acid substrates (Beopoulos et al., 2008; Luo et al., 2002). For instance, the main oxidase *POX2* accomplish the primary step of β-oxidation specifically on medium to long chain fatty acids, C_8-C_{18} (Luo et al., 2002), whose mutation was reported to increase the accumulation of relatively long-chain fatty acids, namely $C_{14:1}$, $C_{18:1}$ and $C_{20:1}$ fatty acids (Mlíčková et al., 2004).

In this work, single and combined mutations involving *MFE1*, *PEX10* and *POX2* were constructed aiming at increasing lipid titers and selectively inhibiting fatty acid degradation to favor C_{18} accumulation, especially $C_{18:1}$, as previously reported in literature (Knothe, 2008; Kinney and Clemente, 2005). Interestingly, our results showed that the combinations of mutations resulted in variations in the lipid composition and favored lipid accumulation to at least 20 % dry cell weight (DCW), compared to 15 % in PO1f with the highest lipid accumulation observed in the single mutant *mfe1*Δ (30 %). All mutants displayed a higher proportion of unsaturated and polyunsaturated fatty acids as well as in a significant decrease in oleic ($C_{18:1n\text{-}9}$), stearic ($C_{18:0}$) and palmitic ($C_{16:0}$) acids compared to the parent PO1f strain. Using regression models, the *in silico* predicted properties and performances of FAME (biodiesel) variants, when used as B100 (100 % unblended biodiesel), were found to meet the ASTM and EN biodiesel standards and most importantly were found to have improved cold flow properties.

As such, this study is laying the foundations for the production of "Genetically Engineered Biodiesel (GEB)" involving the rational

engineering of single cell oil composition to be used as tailor-designed feedstock oils for production of designer biodiesel with improved properties and performances when used unblended.

2. Material and methods

2.1. Strains and growth conditions

Y. lipolytica PO1f double auxotroph (*MATa leu2-270 ura3-302 xpr2-322 axp1-2*) (ATCC no. MYA-2613) and its derivatives were grown from −80 °C stocks in precultures composed of 3 mL of Yeast-Peptone-Dextrose broth (YPD; BioBasic, Canada) in 15 mL-test tubes placed in a rotary drum at 70 rpm and incubated at 28 °C. The mutants *Y. lipolytica* PO1f *mfe1*Δ (*MATa xpr2-322 axp1-2 leu2-270 ura3-302 mfe1*Δ), *pex10*Δ (*MATa xpr2-322 axp1-2 leu2-270 ura3-302 pex10*Δ), *mfe1*Δ-*pex10*Δ (*MATa xpr2-322 axp1-2 leu2-270 ura3-302 mfe1*Δ *pex10*Δ), *pex10*Δ-*pox2*Δ (*MATa xpr2-322 axp1-2 leu2-270 ura3-302 pex10*Δ *pox2*Δ) and *mfe1*Δ-*pex10*Δ-*pox2*Δ (*MATa xpr2-322 axp1-2 leu2-270 ura3-302 mfe1*Δ *pex10*Δ *pox2*Δ) were generated in this study. Transformants were selected on synthetic minimal media containing Yeast Nitrogen Base YNB without amino acids 1.7 g/L ($YNB_{w/o.aa}$; Bio Basic), glucose 20 g/L (BioBasic), ammonium chloride 5 g/L (BioBasic), uracil 0.076 g/L (BioBasic), agar 15 g/L (BioBasic) and phosphate buffer 25 mM, pH 6.8. Plates were incubated at 28 °C for at least 2 days until colonies were well developed. *Starmerella bombicola* Y-5391 (ATCC no. 22214), *Cutaneotrichosporon curvatus* YB-775 (ATCC no. 10567), *Rhodotorula toruloides* Y-6987 (NRRL Y-6987) and *Lipomyces starkeyi* Y-11561 (NRRL Y-11561) were grown from −80 °C stocks in precultures composed of 3 mL of YPD broth (BioBasic, Canada) in 15 mL-test tubes placed in a rotary drum at 70 rpm and incubated at 28 °C.

Y. lipolytica strains were grown for 48 h unless otherwise specified in lipogenic medium YNB glycerol:ammonium chloride (50: 4 g/L, achieving a 22 C/N ratio) composed of $YNB_{w/o.aa}$ 1.7 g/L, glycerol 50 g/L, ammonium chloride 4 g/L, uracil 0.076 g/L, leucine 0.3 g/L (BioBasic) were supplemented as necessary. Medium was also supplemented when specified with additional ammonium chloride 2 g/L (total of 6 g/L) and/or yeast extract 1 g/L (Fisher Scientific, Canada). *S. bombicola* Y-5391, *C. curvatus* YB-775, *R. toruloides* Y-6987 and *L. starkeyi* Y-11561 were grown for 48 h in supplemented YNB glycerol:ammonium chloride (50: 6 g/L) yeast extract 1 g/L.

Cas9 plasmid (Leu^+) were cured from positive transformants by growing isolated colonies in YPD broth 30 °C for 1–2 days. Complete curing of plasmids was achieved after 1–2 subcultures of subclones on YPD. Subcultures were then streaked on YPD agar and isolated colonies were further streaked on YNB-Ura^+-Leu^- to verify complete loss of Leu^+ plasmids.

E. coli DH5*α* strains containing plasmid were grown in Luria-Bertani broth (LB, BioBasic, Canada) supplemented with carbenicillin (50 μg/mL) for plasmid maintenance at 37 °C in a rotary drum.

2.2. Plasmids and oligonucleotides

The plasmids constructed and used in this study are listed in Table 1.

2.3. DNA cloning and gene assembly

Using our previously established protocols (Abdel-Mawgoud and Stephanopoulos, 2020; Ouellet and Abdel-Mawgoud, 2023), the CRISPR plasmid pAS252 was constructed by the ligation of the BsmBI-linearized pAS242 with the thermally annealed oligonucleotides 278(fwd)/279 (rev) forming the $gRNA_{MFE1}$. The CRISPR plasmids pAS207 and pAS199 were constructed from the ligation of the AvrII-linearized pAS164 with the thermally annealed 336(fwd)/337(rev) and 314(fwd)/315(rev) forming the $gRNA_{PEX10}$ and $gRNA_{POX2}$, respectively (Table 2).

Plasmids were transformed into *E. coli* DH5*α* by transferring 100 ng of DNA to 25 μL of competent cells incubated on ice 30 min followed by 45 s of a 42 °C heat shock followed by a 5-min incubation on ice. Cell recovery was made by adding 20 volumes of LB broth followed by incubation of transformation suspension at 37 °C for 45 min. Transformants were concentrated to a volume of 100 μL by centrifugation then plated on LB agar supplemented with carbenicillin 100 μg/mL.

Table 1
List of plasmids and their harboring *E. coli* strains.

Code of plasmid [Code of *E. coli* Strain]	Name	Genotype	Ref.
pAS164 [AS507]	pCRISPRyl-no gRNA- $P_{UAS1B_8\text{-}TEF(136)}$-Cas9	$P_{UAS1B_8\text{-}TEF(136)}$-Cas9-$T_{CYC1}$ $P_{SCR1'}$-tRNA-$sgRNA_{empty}$ *CEN1 LEU2* AMP^R *ColE1*	(Ouellet and Abdel-Mawgoud, 2023)
pAS199 [AS547]	pCRISPRyl-*POX2*-gRNA-*LEU2*	$P_{UAS1B_8\text{-}TEF(136)}$-Cas9-$T_{CYC1}$ $P_{SCR1'}$-tRNA-$sgRNA_{POX2}$ *CEN1 LEU2* AMP^R *ColE1*	This study
pAS207 [AS555]	pCRISPRyl-*PEX10*-gRNA-*LEU2*	$P_{UAS1B_8\text{-}TEF(136)}$-Cas9-$T_{CYC1}$ $P_{SCR1'}$-tRNA-$sgRNA_{PEX10}$ *CEN1 LEU2* AMP^R *ColE1*	This study
pAS242 [AS590]	pCRISPRyl-gRNA empty-*LEU2*-$P_{TEF(366)\text{-}Kozak}$-Cas9	$P_{TEF(366)\text{-}Kozak}$-Cas9-$T_{CYC1}$ $P_{SCR1'}$-tRNA-no sgRNA *CEN1 LEU2* AMP^R *ColE1*	(Ouellet and Abdel-Mawgoud, 2023)
pAS252 [AS600]	pCRISPRyl-*MFE1*-gRNA-*LEU2*	$P_{TEF(366)\text{-}Kozak}$-Cas9-$T_{CYC1}$ $P_{SCR1'}$-tRNA-$sgRNA_{MFE1}$ *CEN1 LEU2* AMP^R *ColE1*	This study

2.4. Yeast transformation

Transformation of *Y. lipolytica* PO1f was carried out using a LiAc/ssDNA/PEG protocol (Abdel-Mawgoud and Stephanopoulos, 2020). A volume equivalent to 1,000 μL.OD was collected from an overnight culture grown in YPD at an OD_{600} between 10 and 15. Cells were centrifuged at 22,000 g for 1 min, washed twice with 50 μL of lithium acetate solution (100 mM, pH 6.0), then suspended in 100 μL of transformation mix (PEG-3350 45 % w/v (Sigma-Aldrich, Canada); lithium acetate 0.1 mM (Sigma-Aldrich); DL-dithiothreitol 0.1 mM (Fisher Scientific, Canada)) and incubated on ice for 15 min. A volume of 2.5 μL of salmon sperm DNA (10 mg/mL) was added together with 1 μg of respective pCRISPRyl (Cas9/gRNA) and deletion allele constructed by Overlap Extension PCR of respective pair of oligonucleotides (Tables 1 and 2). Transformation mixes were incubated 30 min at 28 °C then thermally shocked at 39 °C for 30 min. Cell suspensions were plated on selective $YNB_{w/o.aa}$-Ura^+ minimal media and incubated for at least 2 days at 28 °C until the development of colonies.

2.5. Colony-PCR for screening of transformants

The *Y. lipolytica* transformants were screened using colony-PCR. A biomass of roughly 1 mm^2 was picked and suspended to homogeneity in 10 μL of NaOH 20 mM and lysed at 98 °C for 15 min. A volume of lysates not exceeding 10 % of the total PCR reaction volume was added to the respective PCR mix. Screening of correct clones was conducted with multiplex PCR using the sets of primers 300(Fwd)/301(Rev), 471(Fwd)/472(Rev) and 292(Fwd)/293(Rev) (Table 2) for screening for *mfe1*Δ, *pex10*Δ and *pox2*Δ mutants respectively. All of which was done using the Phire Hot Start II DNA Polymerase (Thermo Fisher Scientific).

2.6. Nile red quantification of lipids

Total lipids were measured using our previously standardized high throughput Nile red quantification protocol (Ouellet et al., 2023). *Y. lipolytica* strains were inoculated from YPD-grown precultures at an

Table 2
List of oligonucleotides.

No	Name	Sequence	Ref.
278	278-*MFE1*gRNA-F	cgcaagtctcaccgaaaccaacca	This study
279	279-*MFE1*gRNA-R	aaactggttggtttcggtgagact	This study
282	282-*POX2*g-del-F	tatataccaaagggatgggtcctcaaaaatcacacaagcaacgacgccatgtagacaagc	This study
283	283-*POX2*-del-R	ttgcaatcaatacataatctttattcatacaataaataacccgcttgtctacatggcgtcg	This study
290	290-*MFE1*-del-F	atttcttaaaatttacttaactcgtatcacttggtcagataatagcttacattgtgtgtg	This study
291	291-*MFE1*-del-R	acgttattaacacaatctatttattcaacacacacacacaatgtaagctattatctgacc	This study
292	292-F-*POX2*	cggctctcggtatttcacat	This study
293	293-R-*POX2*	ggcgtctggtgtagttggtt	This study
300	300-F-*MFE1*	gcagtacacagcgcgataca	This study
301	301-R-*MFE1*	tttcgtaggtcatgccgttt	This study
314	314-F-*POX2*-gRNA-Schwartz	cgcaggttgacgtgcatagacataggccagaag	(Schwartz et al., 2016)
315	315-R-*POX2*-gRNA-Schwartz	aaaccttctggcctatgtctatgcacgtcaacc	(Schwartz et al., 2016)
336	336-F-*PEX10*-gRNA	cgcatacaaggaggagctggaga	This study
337	337-R-*PEX10*-gRNA	aaactctccagctcctccttgta	This study
466	466-*PEX10*-del-F	acgccacgtctgcttactaagcaacccaaatctgcctcggctcaaaatgtaatgacgagg	This study
467	467-*PEX10*-del-R	gatgctctgtgtctcgctgactagtccttccatccagacctcgtcattacattttgagcc	This study
471	471-F-*PEX10*-up	acccaacaacctctccaaca	This study
472	472-R-*PEX10*-dn	gaattggtcgtgtctggtcc	This study

Table 3
Relation between chemical structure of FAMEs (biodiesel) and their combustion and emission performances.*

		DO	C_X	DU
Physico-chemical and combustion related properties	CN	▲	▲	▼
	Heating value	▼	▲	▼
	Viscosity	▲	▲	▼
	Density	▲	▼	▲
	Volatility	▼	▼	▲
	CP	▲	▲	▼
	PP	▲	▲	▼
	CFPP	▲	▲	▼
Emission properties	NO_x	▲	▼	▲
	CO	▼	▲	▲
	UHC	▼	▲	▲
	PM	▼	▲	▲

*The direction of triangles denotes direct (upward triangle) or inverse proportionality of change of biodiesel properties with changing the chemical composition. The color of the triangles indicates whether the direction of change is desired (green) or undesired (red).
CFPP: Cold Filter Plugging Point.
CN: Cetane Number.
CO: Carbon monoxide.
CP: Cloud Point.
C_X: Carbon chain length.
DO: Degree of Oxygenation.
DU: Degree of Unsaturation.
NO_X: Nitrogen Oxides.
PM: Particulate Matters.
PP: Pouring Point.
UHC: Unburnt Hydrocarbons.

initial OD_{600} of 0.1 in test tubes containing 3 mL lipogenic YNB glycerol: ammonium chloride (50: 4 g/L) broth for 48 h. Cells were diluted in 25 mM sodium Phosphate Buffer (PB) pH 6.8, to achieve an OD_{600} falling between 2 and 6 in a final volume of 200 μL on 96-well plates. A volume of 20 μL of Nile red 100 μg/mL (TCI America) in acetone (Fisher Scientific, Canada) was added onto each sample wells for a final Nile red concentration of 10 μg/mL. Plates were sealed with adhesive films and incubated for 30 min at 60 °C while shaking. Fluorescence readings were measured at excitation/emission wavelengths of 544/678 nm using fluorescence plate reader (Fluoroskan Ascent, Thermo Fisher Scientific). Controls accounting for the intrinsic fluorescence of Nile red and cells

Table 4
Standard biodiesel properties defined by the ASTM D6751 and EN 14214.

Properties	ASTM specifications[a]		EN specifications[b]	
	Analysis methods	ASTM D6751-23a	Analysis methods	EN 14214
Flash point (°C)	D93	≥93	ISO 2719	≥101
Kinematic viscosity at 40 °C (mm^2/s)	D445	1.9–6.0	ISO 3104	3.5–5.0
Cetane number	D613	≥45	ISO 5165	≥51
Cloud point (°C)	D2500	–	23015	–
OSI (hrs)	EN 15751	≥3	14112	≥8
Density at 15 °C (g/cm^3)	–	–	ISO 3675	0.86–0.9
Sulfur (%)	D5453	≤0.05	ISO 20846	≤0.001
Phosphorus (%)	D4951	≤0.001	EN14107	≤0.0004
Total glycerin (%)	D6584	≤0.240	EN 14105	≤0.25
Methanol (%)	EN 14110	≤0.2	EN 14110	≤0.2
Additives (%)		≤1.5	–	–

[a] ASTM D6751: This is the international standard specification for biodiesel fuel blend stock (B100) for middle distillate fuels.
[b] EN 14214: This is the European standard specification published by the European Committee for Standardization.

autofluorescence were prepared respectively by adding the Nile red onto 200 μL of PB and by adding acetone instead of Nile red onto cell samples. Dry cell weight (DCW) was measured by weighing dried cells collected from 2 mL of cultures and washed twice in PB before drying in pre-weighed 2 mL microtubes.

2.7. Lipid analysis by GC-FID-MS

Lipids of *Y. lipolytica* strains were extracted and derived in FAMEs using an *in situ* transesterification protocol developed from Van Wychen et al., (2016) and adapted for yeasts by Ouellet et al. (2023). *Y. lipolytica* strains were inoculated in test tubes of 3 mL lipogenic YNB glycerol: ammonium chloride (50: 4 g/L) broth for 48 h as for the Nile red quantification. The equivalent of 5,000 OD•μL of cultures were transferred to 1.5 mL screw-capped GC-vials. Cells were pelleted and washed twice with 1 mL of 25 mM PB. Cells were dried at 60 °C for at least 4 h. A volume of 10 μL of C13:0 methyl ester (10 mg/mL; Fisher Scientific, Canada) were added as internal standard followed by 200 μL of chloroform:methanol 2:1 v/v (Fisher Scientific, Canada) and 300 μL of 0.6 M HCl:methanol (Fisher Scientific, Canada). Vials were sealed with screw caps, mixed and incubated at 85 °C for 1 h. 1 mL of HPLC grade hexane (Fisher Scientific, Canada) was added to cooled down vials then thoroughly vortexed for 10 seconds. Vials were then centrifuged at 22,000 g

for 10 min to induce phase separation. The upper hexane layer was then transferred to a new 1.5-mL GC-vial for GC analysis. Dry cell weight (DCW) was measured by weighing dried cells collected from 2 mL of cultures and washed twice in PB before their drying in pre-weighed 2 mL microtubes.

A volume of 1 μL was injected in a GC-FID (Trace 1300 Gaz chromatograph system, Thermo Fisher Scientific) equipped with a TraceGOLD TG-5MT metal capillary column (ID of 0.25 mm, length of 30 m, film thickness of 0.25 μm composed of (5 %-phenyl)-methylpolysiloxane; Thermo Fisher Scientific) with the following settings: Injector Temperature = 280 °C, Carrier gas (Helium) Flow = 1 mL/min, Oven = 50 °C for 1 min, increased by 25 °C/min to 180 °C, hold 2 min, increased by 0.5 °C/min to 190 °C. increased by 10 °C/min to 350 °C, increased by 25 °C/min to 380 °C and hold 2 min. FID detector was set to 380 °C with hydrogen, air as well as nitrogen as makeup gas flows at 40 mL/min, 450 mL/min and 30 mL/min, respectively. All GC gases were 99.999 % purity (Linde, Canada).

A 30 components FAME standard C8-24 (461-C, Nu Chek Prep, USA) was used for the construction of the calibration curves. The FAME range was extended to C2:0 acetic acid (Thermo Fisher Scientific), C4:0 butanoic acid (Sigma-Aldrich), C5:0 pentanoic acid (Thermo Fisher Scientific), C6:0 hexanoic acid (Sigma-Aldrich) and C7:0 heptanoic acid (TCI) derived in FAMEs. Peak identities were confirmed by GC–MS equipped with an ISQ 7610 Single Quadrupole Mass spectrometer based on electron impact ionization (Thermo Fisher Scientific). A TraceGOLD TG-5MT metal capillary column and the same GC conditions while compensating for vacuum to maintain a carrier gas flow of 1 mL were used. A biodiesel matrix blank (Cat. No. SXBF-BLKX, Spex CertiPrep) was used as a standard of biodiesel composition and properties. Calibration and detection parameters used for fatty acid (FAME) analysis by GC-FID analysis of different are listed in Table S3.

2.8. Data sets and design of experiments for FAME property predictions

Physical and combustion properties of FAME mixtures were predicted using linear regression models (Table 5). Models developed by Su et al. (2011) were used for predicting cetane number (CN) and flash point ($^{\circ}T_{Flash}$) whereas models developed by Ramirez-Verduzco et al. (2012) were for kinematic viscosity (μ), density (ρ) and heating value (HV). Cold flow properties described by the Clouding Point (CP), Pour Point (PP) were predicted by the models of Dunn (2015) and by the Cold Filter Plugging Point (CFPP) predicted using the linear regression in this study. The linear regression was defined from a large set of compiled experimental data from Gomez-Rodriguez et al. (2021), Santos et al. (2023) and Yuan et al. (2017) (Table S4) using the method of least squares by Minitab software (version 17.1.0). The correlation allowing the conversion of MW_{FAME} to C_X and the one allowing to convert $\%U_{FAME}$ to a relation between C_X and N_{DB} were obtained similarly using least squares regression by Minitab software (version 17.1.0) and the same dataset (Table S4). C_X is the weighted-average carbon chain length of the biodiesel ($C_X = \sum_{i=1}^{N}(C_{Xi} \times \%\,\text{abundance of methyl ester})$) and N_{DB} is the unsaturation degree defined by the weighted-average number of double bonds of the biodiesel ($N_{DB} = \sum_{i=1}^{N}(N_{DBi} \times \%\,\text{abundance of methyl ester})$). MW_{FAME} is the weighted-average molecular weight ($MW_{FAME} = \sum_{i=1}^{N}(MW_i \times \%\,\text{abundance of methyl ester})$. The last three parameters are calculated by summing the multiplication products of each parameter (N_{DB}, C_X or MW) of each individual fatty acid by its relative abundance in a pool of fatty acids (whose number is from $i = 1$ to N, where N is the total number of different fatty acids) of an oil. The $\%U_{FAME}$ is the percentage of unsaturated fatty acids (whether mono- or poly unsaturated).

In silico optimisation of FAME properties was performed with a full central composite design using Minitab software (version 17.1.0) and designed with 2 continuous factors: C_X and N_{DB}, star point value (α) of 1.41421. C_X values were fed as 12, 13.76, 18, 22.24 and 24 whereas N_{DB} were 0, 0.44, 1.50, 2.56 and 3 corresponding respectively to the coded values -α, −1, 0, 1 and α. This resulted in a total of 65 runs of 20 cube points, 25 center points and 20 axial points. Data of biodiesel compositions were manually generated respecting the net C_X and N_{DB} proposed by the model design and while introducing due differences in the specific compositions of individual fatty acids of each oil (run). Biodiesel properties (CN, T°_{Flash}, μ, ρ, HV, CP, PP and CFPP) were then calculated for each manually generated biodiesel as a function of C_X and N_{DB} using corresponding mathematical models (Tables 5, S5, and S6). ANOVA statistical analysis was performed on full factorial regression for forward and backward elimination of terms with an $\alpha = 0.05$ (Table S7).

Table 5
Models for prediction of biodiesels properties.

Equation	Property	Model equation	Ref.
(1)	Cetane number (CN)[a]	$CN = 3.93\,(N_C) - 15.936\,(N_{DB}) = 3.93\,(C_x + 1) - 15.936\,(N_{DB})$	(Su et al., 2011)
(2)	Flash Point (T°)[a]	$T^{\circ}_{Flash}(K) = 23.362\,(N_C) + 4.854\,(N_{DB}) = 23.362\,(C_x + 1) + 4.854\,(N_{DB})$	(Su et al., 2011)
(3)	Kinematic viscosity (μ) at 40 °C	$\ln(\mu)\,(mm^2s^{-1}) = -12.503 + 2.496\ln(MW_{FAME}) - 0.178\,(N_{DB})$	(Ramirez-Verduzco et al., 2012)
(4)	Density (ρ) at 20 °C[b]	$\rho(g/cm^3) = 0.8463 + (4.9/MW_{FAME}) + 0.0118\,(N_{DB})$	(Ramirez-Verduzco et al., 2012)
(5)	Heating Value (HV)	$HV\,(MJ/kg) = 46.19 - (1794/MW_{FAME}) - 0.21\,(N_{DB})$	(Ramirez-Verduzco et al., 2012)
(6)	Cloud Point (CP)	$CP(^{\circ}C) = CFPP + 4.5$	(Dunn, 2015)
(7)	Pour Point (PP)	$PP(^{\circ}C) = 0.98\,(CFPP) - 0.69$	(Dunn, 2015)
(8)	Cold Filter Plugging Point (CFPP)[c]	$CFPP(^{\circ}C) = -0.004312\,(\%U_{FAME})^2 + 0.52026\,(MW_{FAME}) - 125.24415$	(This study)
(9)	MW_{FAME} to C_X[d]	$MW_{FAME} = 13.514(C_x) + 52.535$	(This study)
(10)	$\%U_{FAME}$ to C_X, N_{DB}[e]	$\%U_{FAME} = C_X/(0.102606/N_{DB} + 0.136413)$	(This study)

[a] Those equations were described by the factor N_C which is the weighted-average number of carbons on the FAME including the methyl ester group. For our study we used however the C_X that is the N_C minus the methyl ester group such that C_X represents directly the length of fatty acid chain itself. To account for the difference, a + 1 constant was added to C_X so that $N_C = C_X + 1$.

[b] Density can be corrected at 15 °C by applying a factor of 0.9958 (Gov. Canada, 2018).

[c] Determination coefficient of this model is of 0.0.757 And standard deviation is of 3.24 °C.

[d] This equation is for conversion of MW_{FAME} to C_X and can be substituted in equation (3), (4), (5), (8) and (10) to use C_X, a more structurally descriptive term than MW_{FAME}. Determination coefficient is of 0.996 and standard deviation is of 0.826 g/mol (Fig. S1B).

[e] This equation is for conversion of $\%U_{FAME}$ to a relation of MW_{FAME} and N_{DB} and can be substituted in equation (8). In combination with equation (9), it allows to replace $\%U_{FAME}$ with more structurally descriptive terms. Determination coefficient is of 0.735 and standard deviation is of 6.23 %.

3. Results and discussion

3.1. Developing a model for prediction of biodiesels cold filter plugging point

Although biodiesels show clear advantages over petrodiesels, they

are limited however in terms of their cold flow properties and in being associated with higher NO_X emissions. These limitations makes them imperfect alternatives to petrodiesel, especially in cold climates.

Few models, based on experimental data, were reported to predict the cold flow properties as the cloud point, the pour point and, especially, the cold filter plugging point as a function of the palmitic acid methyl ester content, the unsaturation or saturation content, specific methyl esters and other chemistry related metrics (Santos et al., 2023). Though reported models have high predictive power, yet each model of which remains valid only within the limited range of the specific fatty acid compositions of oils that were used for developing each model. Many were hardly applicable to highly saturated, very short chain, or very long chain FAME. Therefore, it was necessary to develop an overall regression model based on available experimental cold filter plugging point (CFPP) data, yet, of a larger pool of FAMEs (biodiesels) belonging to a wide range of different oils with diverse fatty acid compositions. To do so, reported experimental CFPP data were compiled from the work of Gomez-Rodriguez et al. (2021), Santos et al. (2023) and Yuan et al. (2017) which made a total of 379 plant and animal oils including blends of these along with their specific fatty acid composition (Table S4). Compiled data were used to develop a linear regression model to predict CFPP as a function of average molecular weight (MW_{FAME}, which is the weighted average MW) and unsaturated content of FAME ($\%U_{FAME}$, which is the percentage of fatty acids containing double bonds, irrespectful of their number in each fatty acid) (Equation 8).

$$\text{CFPP}\ (^{\circ}\text{C}) = -0.004312\ (\%U_{FAME})^2 + 0.52026\ (MW_{FAME}) - 125.24415 \quad (8)$$

The CFPP regression model (Equation 8) showed to be significantly linear (Fig. S1A) and to have a comparable predictive power to those previously reported models generated from sub data sets Gomez-Rodriguez et al. (2021), Santos et al. (2023) and Yuan et al. (2017) (Table S1). Nonetheless, the model of this study is valid and accurate over a wider range of FAME chemical compositions (covering unsaturated content at as low as 7 % and as high as 95 %). Moreover, previously reported models were dependant solely on the unsaturated content as variable (Su et al., 2011; Sarin et al., 2010) which makes them of less predictive accuracy for biodiesels with high saturated content, the fact this was corrected in the CFPP model of this study. Therefore, the CFPP regression model of this study was adopted for CFPP prediction. For other biodiesel metrics, previously reported models were used as mentioned later.

3.2. *In silico* prediction of optimal FAME compositions using DOE

The optimal FAME composition was predicted, using *in silico* models, to be used as the target composition of a "designer" biodiesel having optimal properties and performance characteristics to be sought in this study. This target chemical composition was then the goal of the genetic engineering of oleaginous yeasts used for production of designer biodiesel.

To do so, full factorial central composite design was applied aiming at finding the optimal FAME compositions within the range of a carbon chain length (C_X) from 12 to 24 carbons and a weighted-average number of double bonds (N_{DB}) from 0 (saturated) to 3. The tested ranges of C_X and N_{DB} were arbitrarily selected from within composition ranges of vegetable oils and such that to be biologically achievable in microbial platforms like, *Y. lipolytica*. The factors C_X and N_{DB} were selected as the independent variables or factors as they are better structural descriptors of FAMEs compared to the average molecular weight (MW_{FAME}) or percentage of unsaturated content ($\%U_{FAME}$) though they intercorrelate very well (Fig. S1B, S1C). The N_{DB} range (0 to 3) was inspired based on N_{DB} values in plant-based biodiesels whose lowest and highest known unsaturation degrees are 0.1 for coconut (Serrano et al., 2014) and 2.7 for tung biodiesels (Yuan et al., 2017), respectively. For the C_X range, it was centered at 18 ± 6 carbons of length (C_{18} being the major fatty acid in *Y. lipolytica*) which also includes extremes of C_X values in plant-based biodiesels with the shortest and longest carbon chain lengths, namely coconut oil ($C_X = 12.1$) (Serrano et al., 2014) and pennycress ($C_X = 19.3$) (Moser, 2014).

The central composite design generated 65 runs including quintuplicates, for which different FAME compositions were generated that varied in their C_X and N_{DB} (independent variables or factors) and for which biodiesels properties (dependent variables) were expected and used as responses for the central composite design input data (Table S5). For these runs, 65 different FAME compositions were generated all while making sure to keep the net C_X and N_{DB} values the same within every quintuplicate composition as requested by the central composite design. For each FAME composition, biodiesel properties, namely, cetane number (CN), kinematic viscosity (μ), density (ρ), heating value (HV), flash point (T°_{Flash}), cloud point (CP), pouring point (PP)- and cold filter plugging point (CFPP) were predicted using our model for CFPP (Equation (8), Table 5) and other reported models (Su et al., 2011; Santos et al., 2023; Saxena et al., 2013) (Table 5). Calculated predictions were then fed as responses in the data set for the central composite design (Tables S5 and S6). Model selection for this study was based on predictive accuracy of models and range size of predictors, i.e. limits of FAME composition. Response surfaces of predicted biodiesel properties were generated as a function of FAME compositions, C_X and N_{DB} that demonstrated different regression profiles (Fig. 1). Response surfaces of all biodiesel properties demonstrated mostly linear regression models with uphill or downhill surfaces and slight curvatures (Fig. 1). Over the tested range of studied factors (C_X and N_{DB}), cold flow properties, cetane number and viscosity are significantly dependent on both C_X and N_{DB}, whereas the biodiesel flash point, and heating value, were more dependent on C_X alone, in contrast to biodiesel density that showed to be dependent on N_{DB} alone (Fig. 1).

Zones of response surfaces of biodiesel properties that are complying to ASTM and EN specifications (Table 4), were identified (Fig. 1), taking into account that EN regulations were used for that purpose as they are more constraining than that of ASTM. Response surfaces show a more confined range of FAME composition fulfilling standard specifications of cetane number and kinematic viscosity. This makes them critical properties that require careful consideration during designing a biodiesel composition.

To visualize a combined plot of properties as a function of chemical composition, a composite overlaid contour plot of cetane number (CN), flash point (T°_{Flash}), kinematic viscosity (μ) and density (ρ), using corresponding models (Table 5), was plotted under constraints respecting regulatory specifications where: the cetane number (CN) is ≥ 51, the flash point (T°_{Flash}) ≥ 101 °C, the viscosity (μ) is between 3.5 and 5.0 mm^2s^{-1} and the density (ρ) at 15 °C is between 0.6 and 0.9 g/cm. The composite overlaid contour plot highlights the explorable region of compliance for biodiesel properties and the corresponding ranges of average FAME compositions (C_X and N_{DB}) fulfilling them. From this composite plot, it could be concluded that it is desirable for biodiesel to have an average carbon chain length of 15–21 carbons and degree of unsaturation of 0–2 double bonds. In other words, a biodiesel mainly composed of $C_{16:0}$, $C_{16:1}$, $C_{16:2}$, $C_{18:0}$, $C_{18:1}$ and $C_{18:2}$ would meet the theoretical optimum. This theoretical optimum is concordant with other studies that reported improved biodiesel properties with increased abundance of $C_{18:1}$ (Knothe, 2008; Kinney and Clemente, 2005).

The starting properties of biodiesels generated from lipids of *Y. lipolytica* PO1f were then investigated, in comparison with standard biodiesel B100 (VWR, Cat. No. SXBF-BLKX). Total lipids of PO1f cells grown in YNB glycerol:NH_4Cl (50: 4 g/L) were harvested after 48 h and then transesterified. The FAME composition of PO1f strain, as well as the biodiesel standard B100 compositions were analyzed by GC-FID-MS and their biodiesel properties were predicted using respective models (Table 5). B100 standard was mostly composed of $C_{18:1}$ and $C_{18:2}$ representing 85 % of its total FAMEs whereas the PO1f showed a more

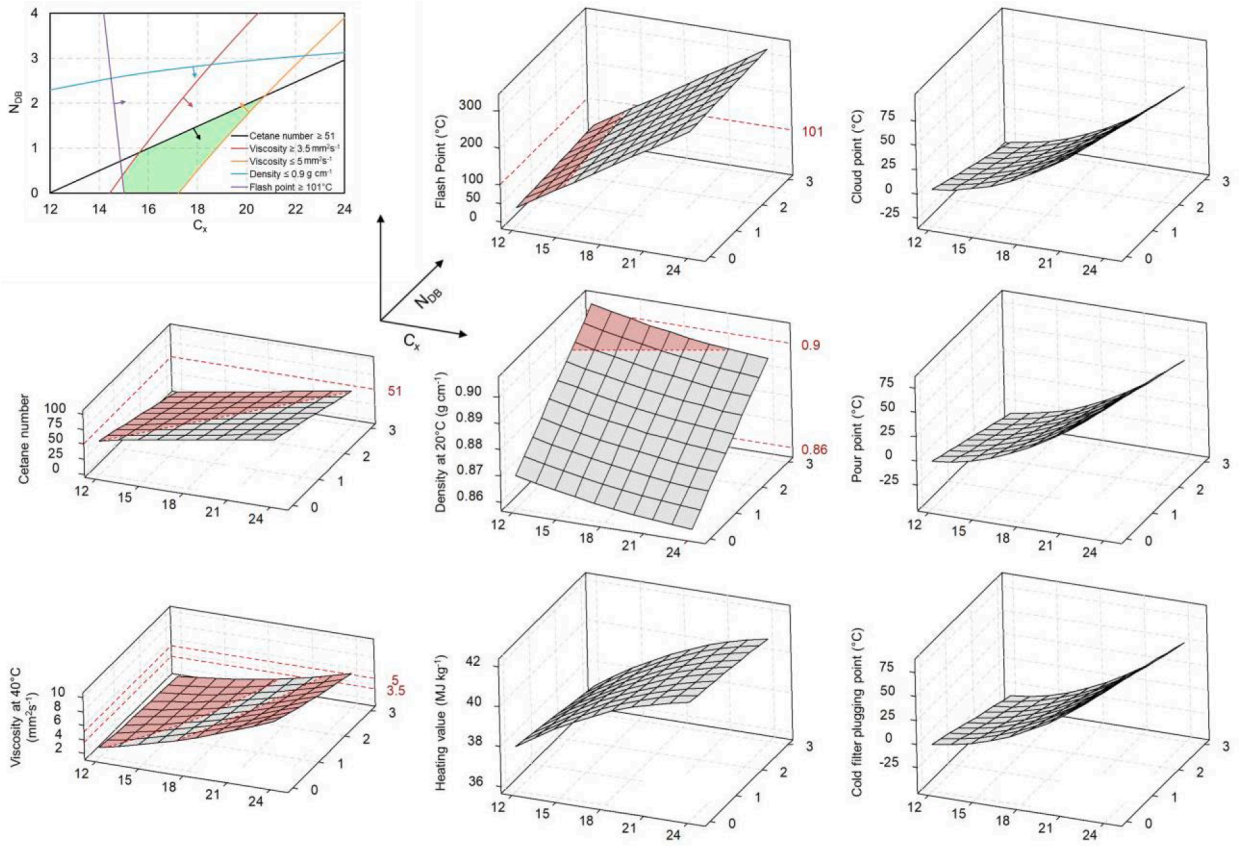

Fig. 1. Statistical optimisation of biodiesel properties in function of average composition. Full-factorial regressions of predicted biodiesel properties in function of C_X and N_{DB} giving response surfaces. Upper and lower limit of ASTM D6751 and EN 14214, the latter was used as it is more constraining, were superposed in red to cetane number, kinematic viscosity, flash point and density response surfaces. Zones complying to EN standards are shown in red overlays. The composite conditional plot (upper left) shows the zone (green) of average FAME composition, based on C_X and N_{DB}, that is complying with ASTM D6751 and EN 14214. (For interpretation of the references to color in this figure legend, the reader is referred to the web version of this article.)

diverse composition with $C_{18:1}$ and $C_{18:2}$ representing 55 % of total FAME (Table S2). Interestingly, the properties of the PO1f biodiesel already meets the ASTM and EN specifications without any genetic manipulation. However, values of its metrics related to cold flow properties were significantly above 0 °C, the fact that incited us to investigate the *in silico* optimization of FAME cold flow properties (CP, PP, CFPP) whilst constraining CN and viscosity (μ) to be in compliance with the EN specification limits.

Compared to B100 standard, FAME composition of PO1f strain was of a lower average chain length ($C_X = 17.48$ compared to 17.80 for the B100 standard) and of a 1.7 times lower average degree of unsaturation ($N_{DB} = 0.87$ for PO1f compared to 1.47 for the B100 standard). The predicted properties of PO1f and B100 biodiesels were strikingly different with respect to cold flow properties (CP, PP, CFPP), cetane number (CN) and viscosity. Compared to B100 biodiesel, the PO1f biodiesel was predicted to have a higher CN (58.77 compared to 50.39), higher kinematic viscosity (4.43 compared to 4.09 mm^2s^{-1}) and less desirable CP, PP and CFPP at 12.26, 6.92 and 7.76 °C, respectively compared to 0.83, −4.29 and −3.67 °C for B100 (Table 7).

Using the optimizer function of Minitab software, the optimal FAME composition associated with optimal cold flow properties (lowest temperatures) was predicted to be at C_X and N_{DB} of 17.36 and 1.33, respectively; this is while constraining the CN to 51 and the viscosity (μ) to 4 mm^2/s at equal weights of importance of 1. Desirability index were of 100, 99.98 and 88.06 respectively for CN, μ and for the three cold flow properties (CP, PP, CFPP). Recalculation of cold flow properties at chemical composition optimum, C_X of 17.36 and N_{DB} 1.33, revealed a CP of −0.1 ± 7.7 °C, a PP of −5.3 ± 7.7 °C and a CFPP of −4.6 ± 7.7 °C taking into consideration that CP and PP require CFPP as independent variable and that the latter requires models (9) and (10) for its calculation using model (8). The mentioned ± 7.7 °C uncertainty is the propagated uncertainties of models (8), (9) and (10).

Table 6
Values of different chemical composition parameters of biodiesels of yeast strains and mutant as well as of biodiesel standard.

	C_X	N_{DB}	$\%U_{FAME}$	MW_{FAME}	SCSF
PO1f	17.48	0.87	63.73	289.32	102.56
*mfe1*Δ	17.31	1.28	78.52	285.32	55.65
*pex10*Δ	16.96	1.20	73.22	280.35	67.55
*mfe1*Δ-*pex10*Δ	17.00	1.21	74.38	280.66	64.10
*pex10*Δ-*pox2*Δ	17.11	1.16	71.50	282.89	75.17
*mfe1*Δ-*pex10*Δ-*pox2*Δ	17.09	1.21	73.78	282.60	68.51
Biodiesel standard	17.80	1.47	84.37	292.67	43.82
R. toruloides Y-6987	17.64	0.60	47.34	292.24	152.23
S. bombicola Y-5391	17.73	0.75	74.98	293.22	73.74
L. starkeyi Y-11561	17.48	0.83	56.65	289.76	122.56
C. curvatus YB-775	17.68	0.96	64.38	292.69	102.96

Given that the native lipid profile of *Y. lipolytica* PO1f ($C_X = 17.48$ and $N_{DB} = 0.87$) is already close to the predicted optimal FAME composition ($C_X = 17.36$ and $N_{DB} = 1.33$), engineering lipids of PO1f to attain an optimal biodiesel composition with improved operability in cold environments while abiding by ASTM and EN regulations is seemingly feasible.

3.3. Lipid accumulation kinetics in different mutants

Different single, double and multiple *Y. lipolytica* mutants defective

Table 7
Predicted properties of biodiesels originating from lipids of mutants constructed in this study.

	CN	μ (at 40 °C)	HV	T°Flash	CP	PP	CFPP	ρ (at 15 °C)
Biodiesel source[a]		($mmyy^2/s$)	(MJ/kg)	(°C)	(°C)	(°C)	(°C)	(g/cm^3)
Y. lipolytica PO1f	58.77	4.43	39.81	162.76	12.26	6.92	7.76	0.870
Y. lipolytica mfe1Δ[b]	51.55	3.98	39.63	160.87	1.11	−4.01	−3.39	0.875
Y. lipolytica pex10Δ	51.46	3.86	39.54	152.32	1.99	−3.15	−2.51	0.874
Y. lipolytica mfe1Δ-pex10Δ	51.36	3.86	39.54	153.16	1.42	−3.71	−3.08	0.874
Y. lipolytica pex10Δ-pox2Δ	52.73	3.98	39.61	155.47	4.39	−0.80	−0.11	0.874
Y. lipolytica mfe1Δ-pex10Δ-pox2Δ	51.76	3.93	39.59	155.43	2.81	−2.35	−1.69	0.874
R. toruloides Y-6987	63.70	4.77	39.93	165.22	21.63	16.10	17.13	0.866
S. bombicola Y-5391	61.66	4.68	39.91	168.08	7.56	2.31	3.06	0.868
L. starkeyi Y-11561	59.42	4.48	39.82	162.52	16.17	10.75	11.67	0.869
C. curvatus YB-775	58.06	4.48	39.86	167.99	13.66	8.28	9.16	0.871
Biodiesel standard	50.39	4.09	39.75	173.11	0.83	−4.29	−3.67	0.877

[a] Biodiesel properties are calculated as 100 % biodiesel (B100).
[b] Biodiesel of this mutant is associated with best biodiesel properties compared to all strains.

in different steps of lipid metabolism were constructed, namely, *mfe1*Δ (multifunctional enzyme catalyzing the hydration/oxidation steps of fatty acids β-oxidation), *pex10*Δ (peroxisome biogenesis factor), and *pox2*Δ (main peroxisome oxidase catalyzing the first oxidation on C_8-C_{18} fatty acids during β-oxidation).

Lipid profiling of constructed mutants was conducted in a standard lipogenic medium with high carbon to nitrogen ratio, YNB glycerol: NH_4Cl (50: 4 g/L), that stimulates lipid accumulation in *Y. lipolytica* (Ouellet et al., 2023) in order to maximize the capacity of detecting minor chemical changes in lipid profile post genetic manipulations. Given that mutant might have different growth kinetics, and that growth phase-specific lipid profile variabilities were to be avoided, growth and lipid kinetics were analyzed beforehand in all strains to be able to harvest cells at the same growth phase for lipid profiling. For all strains, lipid titers were measured at harvest points corresponding to mid logarithmic, late logarithmic and stationary growth phase (Fig. 2) using Nile red quantification of total lipids in the strains PO1f, *mfe1*Δ, *pex10*Δ, *mfe1*Δ-*pex10*Δ, *pex10*Δ-*pox2*Δ and *mfe1*Δ-*pex10*Δ-*pox2*Δ grown in YNB glycerol:NH_4Cl (50: 4 g/L) with 25 mM phosphate buffer.

It was observed that the mid and late logarithmic and stationary phases of growth are respectively at 24, 48 and 60 h, for the reference PO1f strain, yet they are respectively 12, 24 and 48 h for all mutants, i.e. mutants have shorter life cycles (age faster) by about 24 h (Fig. 2A). In addition, at the stationary phase, most mutants attained 45–60 % of the optical density (OD_{600}) attained by PO1f, whereas *mfe1*Δ attained only 22.1 % of that attained by PO1f (Fig. 2A).

Total lipid titers were quantified by Nile red fluorescence and normalized to dry cell weight (RFU/DCW) at the mid and late logarithmic as well as at stationary phases of growth for mutants and PO1f strains (Fig. 2A). Lipid compositions seemed constant across tested time points for every strain with lipid titers that are slightly higher at the late logarithmic phases (Fig. S2). Therefore, for subsequent experiments, lipid titers were compared at the late logarithmic phases in different strains . Consistent with previous reports (Blazeck et al., 2014; Dulermo and Nicaud, 2011; Ng et al., 2020), the mutant *mfe1*Δ demonstrated a lipid content that is three times higher than that of the reference PO1f strain (Fig. 2B). This was followed by the double *mfe1*Δ-*pex10*Δ and the triple *mfe1*Δ-*pex10*Δ-*pox2*Δ mutants whose lipid titers were both slightly more than twice that of PO1f strain (Fig. 2B). On the third rank, the simple *pex10*Δ and double *pex10*Δ-*pox2*Δ mutants had both lipid

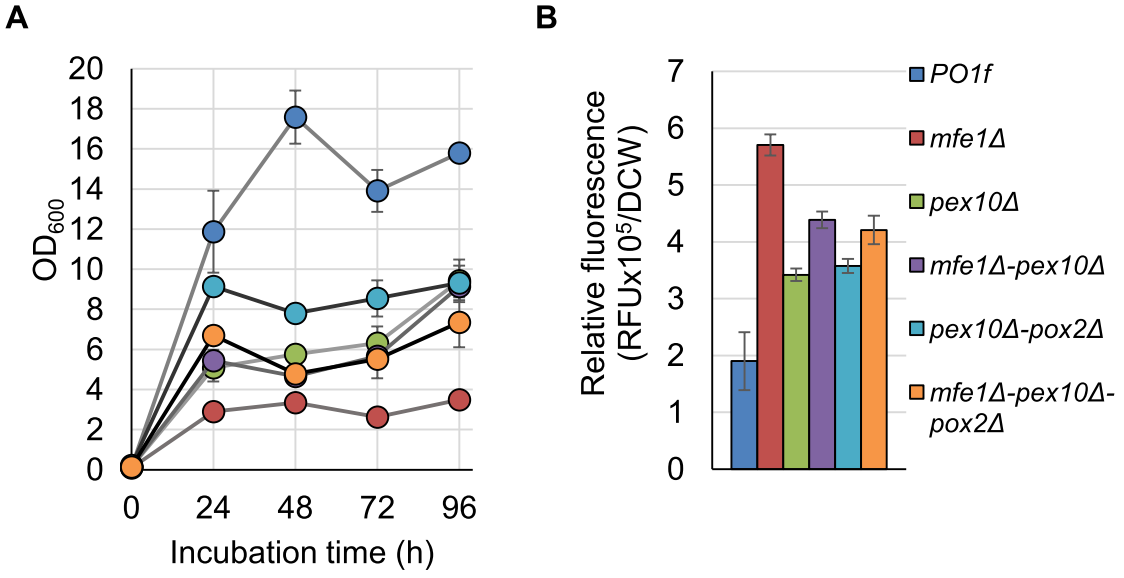

Fig. 2. Growth profiles and lipid titers of mutant and PO1f strains of *Y. lipolytica* in lipogenic medium. (A) Monitoring of strains OD_{600} over 96 h to define their respective growth phases in lipogenic medium: YNB glycerol:ammonium chloride (50: 4 g/L). (B) Lipid titers in terms of Nile red fluorescence normalized to dry cell weight (RFU/g of DCW or RFU/DCW) at late-logarithmic phase (24 hrs for mutants and 48 hrs for PO1f). Lipid titers are reported as the amount of fluorescence per gram of DCW. The mean and the standard deviation of growth and lipid accumulation from 3 biological replicate data are shown. (For interpretation of the references to color in this figure legend, the reader is referred to the web version of this article.)

titers slightly more than twice that of PO1f strain (Fig. 2B). This ranking is concordant with the results of Ng *et al.* (Ng et al., 2020) where the *mfe1*Δ mutation resulted in two times more accumulation of lipids than that in the *pex10*Δ mutant. In contrast, Blazeck *et al.* (Blazeck et al., 2014) reported that the mutants *pex10*Δ and *mfe1*Δ-*pex10*Δ perform equally and even better than the single mutant *mfe1*Δ, nonetheless, important differences in growth medium (with respect to carbon, nitrogen and amino acids sources) between the two studies might explain this discrepancy.

3.4. Lipid compositions in different mutants

Profiling of lipid composition in different mutants was conducted to specifically examine the impact of mutations on fatty acid chain lengths and degree of unsaturation aiming at finding a mutation that achieves the target optimal lipid composition.

Cells were harvested at late logarithmic phases (48 h for PO1f and 24 h for different mutants) and their total lipids were transesterified into FAMEs and analyzed by GC-FID-MS.

Native fatty acid composition in *Y. lipolytica* PO1f showed to be mainly (~72 % of total lipids) comprised of palmitic ($C_{16:0}$), linoleic ($C_{18:2n-6}$) and oleic ($C_{18:1n-9}$) acids (Table S2). In addition, low amounts of the uncommon heptadecanoic ($C_{17:0}$) and heptadecenoic ($C_{17:1n-8}$) acids were also detected in most of the strains (Table S2). Nonetheless, the lipid profile of the mutants differed significantly from that of reference PO1f strain. The mutants in general showed higher relative abundance of shorter saturated fatty acids, namely tetradecanoic ($C_{14:0}$) and pentadecanoic ($C_{15:0}$) acids as well as unsaturated fatty acids, namely palmitoleic ($C_{16:1n-7}$), linoleic ($C_{18:2n-6}$) and vaccenic ($C_{18:1n-7}$) acids, yet with lower amount of both $C_{18:1n-9}$ and $C_{18:0}$ than PO1f strain (Fig. 3). On top of that, the mutants had no detected amounts of 7-hexadecenoic acid ($C_{16:1n-9}$) which was detected in PO1f at 1.2 % (Table S2). Moreover, the total amount of unsaturated fatty acids accounted for more than 70 % of total lipids in mutant strains (~25 % monounsaturated fatty acids (MUFA) and ~47 % polyunsaturated fatty acids, PUFA) compared to 64 % in PO1f strain (41 % MUFA and 23 % PUFA) (Table S2).

Although the lipid profiles of mutant strains are generally close to each other in nature, levels and trend of change of individual fatty acids relative PO1f strain, yet few fatty acids changed differently in *mfe1*Δ compared to other mutants. For instance, *mfe1*Δ did not exhibit remarkable change in $C_{17:1n-8}$ acid but showed higher abundances of $C_{14:0}$, $C_{16:0}$, $C_{18:1n-7}$ and $C_{22:0}$ acids compared to other mutants (Fig. 3, Table S2). For identical mutations in *Y. lipolytica* made by Ng *et al.* (Ng et al., 2020), such variations in the lipid profile were not reported. Blazeck *et al.* (Blazeck et al., 2014) however, noticed a similar increase of C_{16}, C_{17} fatty acids and unsaturated fatty acids in corresponding mutants.

3.5. Attempts to correct growth defects in mutants

Although the lipid profiles of constructed mutants are interestingly richer in unsaturated content which could qualify their oils as feedstocks for the production of novel biodiesel variants, yet they showed growth defects (Fig. 2A) which might affect their economical profitability in industrial contexts. Attempts to optimize the medium components supporting better growth in mutants were conducted. These attempts were motivated by the hypothesis that the nitrogen-limited medium (YNB) used, which is slowing down TCA cycle and stimulating leakage of mitochondrial citrate into cytoplasm to support lipogenesis (Ouellet et al., 2023), should also result in disequilibrium in energy and redox molecules in the cell, and result in slowing down of growth. This disequilibrium might be further accentuated in mutants disrupting lipid degradation, as the latter is one of the palliative pathways re-establishing energy and redox homeostasis. It was then thought that partial supplementation of nitrogen could maintain a small flux in TCA cycle and hence partly correct the impaired growth.

Accordingly, nitrogen content was increased in the basal lipogenic YNB glycerol:NH_4Cl (50:4 g/L) with ammonium chloride (2 g/L) alone or with yeast extract (1 g/L) supplementation. The strains PO1f, *mfe1*Δ and *mfe1*Δ-*pex10*Δ-*pox2*Δ were grown in modified lipogenic YNB broth for 48 h, then lipids were quantified using Nile red fluorescence.

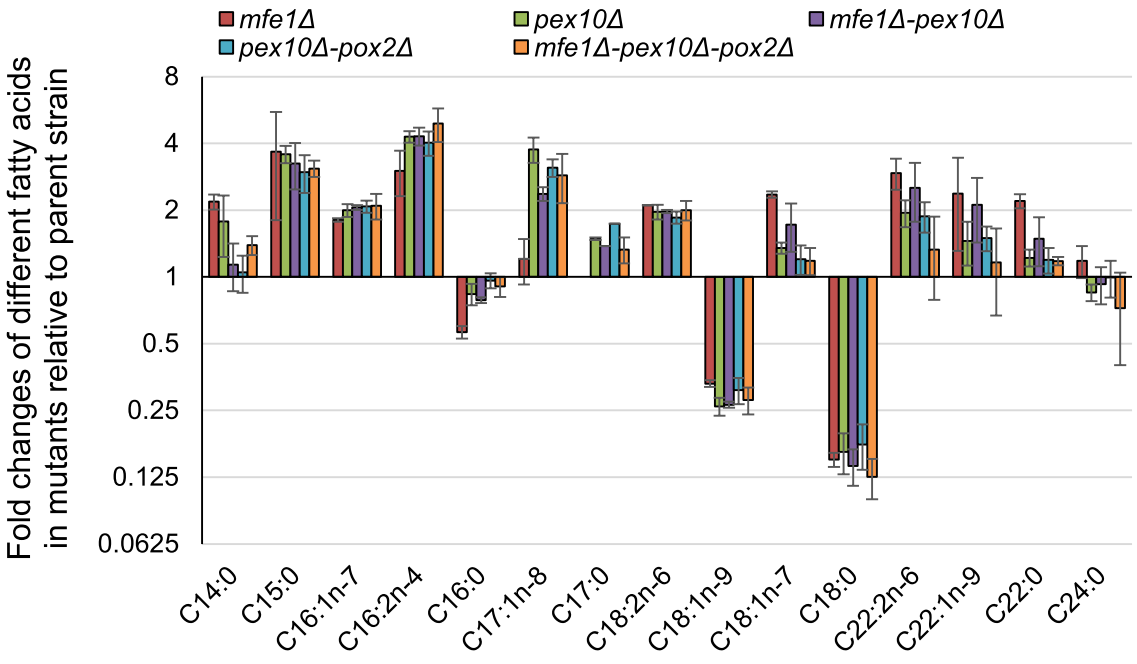

Fig. 3. Fold changes of different fatty acids in mutants relative to parent strain. Relative fatty acid composition of total lipid extract at late-logarithmic phase from mutants relative to PO1f strains grown YNB glycerol:ammonium chloride (50:4 g/L) analyzed by GC-FID. The mean and the standard deviation of lipid profiles from 3 biological replicate data are shown.

Data showed that supplementation of ammonium chloride and particularly yeast extract resulted in a slight decrease in lipid accumulation in the triple mutant with no significant change in PO1f or *mfe1*Δ (Fig. 4A). For growth however, addition of yeast extract to the basal medium (net 4 g/L ammonium chloride and 1 g/L yeast extract) boosted growth of *mfe1*Δ and particularly that of the triple mutant *mfe1*Δ-*pex10*Δ-*pox2*Δ, yet not that of the PO1f. Further increase of nitrogen content on top of yeast extract supplement 1 g/L did not result in further increase of growth of any strain, instead, it resulted in decrease of growth (Fig. 4B). Although supplementation of yeast extract (at 1 g/L) slightly corrected growth defects of simple and triple mutants, yet it came at a price of a significant lowering of their lipid contents. In all nitrogen supplementations tests, growth of mutants was still drastically lower than the parent PO1f strain, denoting that growth defects are not mainly attributed to nitrogen limitation.

It was then hypothesized that the impaired growth of mutants could be attributed to an extensive cell acidification in mutants resulting from high flux of cytoplasmic acetyl-CoA arising from the release of mitochondrial citrate into the cytoplasm and its subsequent conversion into acetyl-CoA ultimately used for lipogenesis upon slowing down of TCA cycle in nitrogen-limited media (Papanikolaou and Aggelis, 2011; Ratledge and Wynn, 2002). Accumulation of citrate when not supported with sufficient ATP and NADH flux required for lipogenesis, might lead acetyl-CoA being transformed into acetate causing cell acidification and growth impairment. To validate this hypothesis, the buffering capacity of the lipogenic medium, YNB glycerol:NH_4Cl (50:4 g/L), was increased by using 50 mM instead of 25 mM phosphate buffer. Strains were grown in both media for 48 h and their total lipid contents were quantified using Nile red fluorescence. Increasing the buffering capacity had no significant change on lipid titers in PO1f or *mfe1*Δ strains yet surprisingly, it had a negative effect on the double, *mfe1*Δ-*pex10*Δ, and triple *mfe1*Δ-*pex10*Δ-*pox2*Δ mutants that accumulated 40 % less lipids. (Fig. 5A). It was reported that *Y. lipolytica* grown on buffered media favors the accumulation of citrate rather than lipids compared to when grown in unbuffered media (Zhao et al., 2015; Nambou et al., 2014).

The pH at the end of incubation was also measured to estimate the extent to which the 50 mM phosphate buffered medium circumvents acidification stress (Fig. 5C, 5D). Increasing the buffering capacity of the medium (using 50 mM instead of 25 mM phosphate buffer) decreased medium acidification by as much as 2 pH units in *mfe1*Δ cultures after 48 h of cultivation yet only by about 0.3 pH units in other strains (Fig. 5C, 5D). This might entail a lower production of free organic acids (or a better conversion of citrate and acetate into lipids) in *mfe1*Δ, compared to other strains, that made *mfe1*Δ unable to lower the pH of stronger buffers. It might also be the slower rate of growth of *mfe1*Δ that explains its lower production of organic acids. As a conclusion, boosting buffering capacity did not correct growth significantly and caused no change or caused a slight decrease in lipid production in mutants (Fig. 5A, 5C). This means that the poor growth observed in mutants stems from factors other than the acidification or phosphate concentration, yet it might be slightly corrected by the supplementation of yeast extract (1 g/L) for the simple (*mfe1*Δ) or triple (*mfe1*Δ-*pex10*Δ-

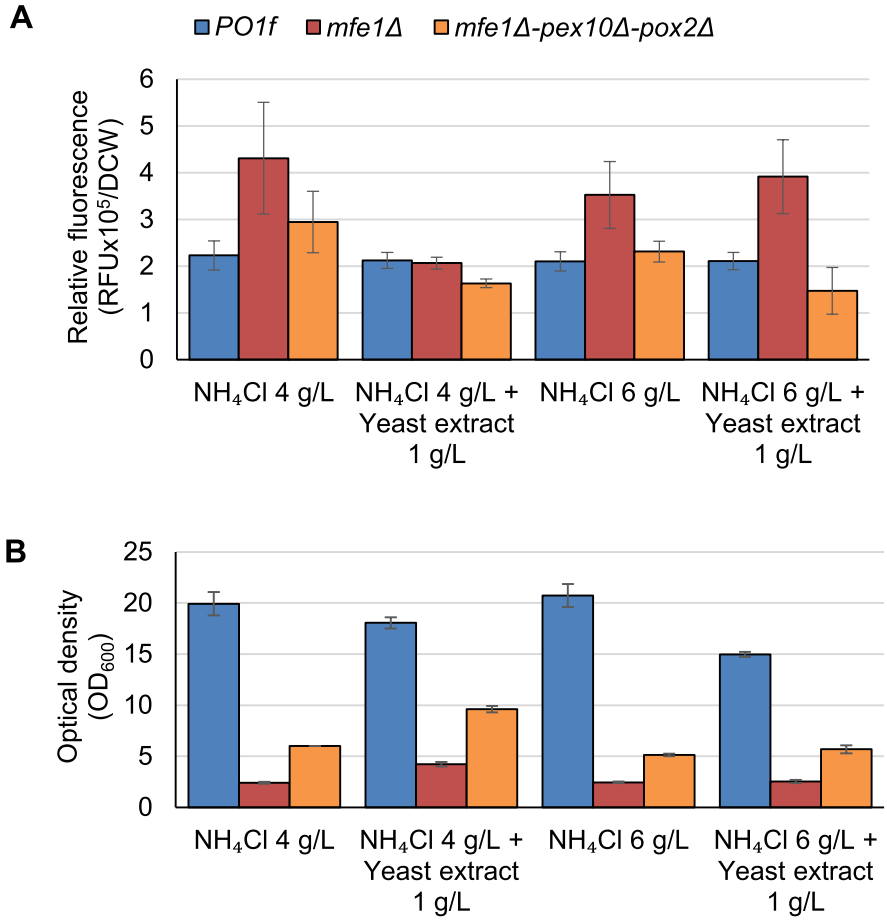

Fig. 4. Monitoring changes of lipid titers and growth of mutants upon modulation of nitrogen content in lipogenic medium. (A) Total lipid titers measured by Nile red fluorescence and (B) growth of mutant and PO1f strains grown in YNB glycerol:ammonium chloride (50: 4 g/L) for 48 h with supplementation of additionnal nitrogen 2 g/L and yeast extract 1 g/L. The mean and the standard deviation of growth and lipid accumulation from 3 biological replicate data are shown. (For interpretation of the references to color in this figure legend, the reader is referred to the web version of this article.)

*pox2*Δ) mutants.

Although increasing the buffering capacity did not change significantly lipid titers, its impact, if any, on lipid composition was examined. Strikingly, PO1f lipid profile demonstrated a shift in lipid composition in 50 mM buffered media (less acidic medium) such that it became similar to that of mutants (shorter chains and higher degree of unsaturation),

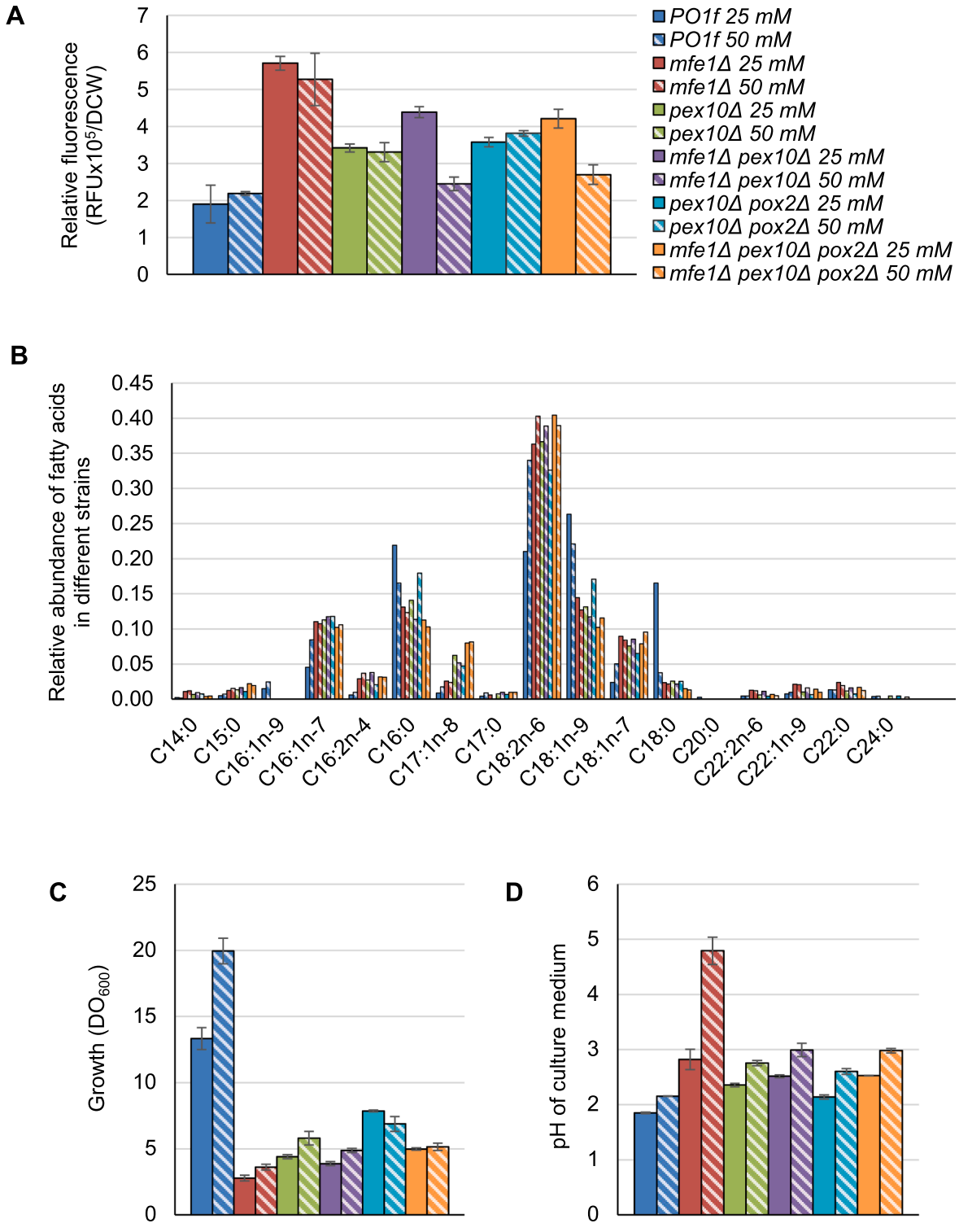

Fig. 5. Lipid titers and profiles in cells grown in 25 mM and 50 mM phosphate buffered medium. In lipogenic medium YNB glycerol:ammonium chloride (50: 4 g/L) buffered at 25 and 50 mM phosphate buffers we show: (A) Lipid titers of mutant and PO1f strains grown for 48 h quantified by Nile red fluorescence. (B) Lipid profiles of total lipids extracted from cells collected at 48 h of mutant and PO1f strains as analyzed by GC-FID and expressed as relative peak abundance of different fatty acids in different strains. (C) Growth of strains as measured by optical density at 600 nm. (D) pH of the liquid culture after 48 h of growth. The mean and the standard deviation from 3 biological replicate data are shown. (For interpretation of the references to color in this figure legend, the reader is referred to the web version of this article.)

yet with certain fatty acids, namely, $C_{16:1n-9}$ that remained only in PO1f and $C_{18:1n-9}$ that was present at higher concentration in PO1f relative to mutants (Fig. 5B). The effect of pH on membrane composition was investigated on the yeast *Candida glabrata* and revealed that the transcription mediator Med15p at pH 2 upregulates lipid elongases and desaturases genes ultimately impacting membrane lipid composition and fluidity by decreasing shorter fatty acids ($C_{16:0}$ and $C_{16:1}$) and increasing longer fatty acids ($C_{18:1}$) (Qi et al., 2017). Similarly, PO1f when grown in weakly buffered media (25 mM, more prone to become acidic medium) showed lower abundance of shorter unsaturated fatty acids (e.g. $C_{16:1n-7}$) yet, higher abundance of longer unsaturated ($C_{18:1}$) and particularly saturated ($C_{18:0}$) fatty acids. Overall, this entails that low pH (resulting from the use of weakly buffered media) might trigger certain cellular stress responses modulating fatty acid composition that results in the biosynthesis of fatty acids of longer chain lengths and of lower degrees of unsaturation in PO1f. The observation that the mutants were not subject to any significant variation in their lipid composition (Fig. 5B) might suggest that mutated genes targeted in this study might be part of cascade of pH-dependent intracellular stress response, and their inactivation blocked any lipid profile change upon change of pH. These results are however attracting the attention towards the possible modulation of lipid profiles by just modulating the composition of the medium.

3.6. Predictions of biodiesel properties of FAMEs of lipids of constructed mutants

The distinct fatty acid profiles of lipid-overproducing mutants incited the study of their derived biodiesels using the same mathematical models (1) to (8) (Table 5). The predicted biodiesel properties of these mutants were then compared to the theoretical optimum as well as to the reference standard biodiesel matrix B100 (Cat. No. SXBF-BLKX).

Predictions revealed a CN above 50 in FAMEs of all strains (Table 7). Mutants-derived biodiesels have CNs that are only 6.6 % (3.85 units) lower than that of the PO1f strain, yet, their CNs are still higher than that of the B100 biodiesel standard by 3.5 % (1.82 units). The *mfe1*Δ mutant has slightly lower CN by only one unit among all strains, yet its CN is more than one unit higher than that of the standard biodiesel B100. This might be explained by the slightly higher unsaturation degree of *mfe1*Δ compared to all strains that is yet slightly less than that of the standard biodiesel B100. Furthermore, biodiesels of mutants exhibited significantly lower viscosities compared to the PO1f, by ~0.4 mm^2/s, and lower to a lesser extent compared to that of the standard biodiesel B100, by ~0.2 mm^2/s. The lower viscosities of mutants-derived biodiesels might be due to their shorter average chain lengths and higher average degrees of unsaturation.

In contrast, the biodiesel densities and heating values did not vary substantially between different FAME variants of this study. In fact, the densities of FAMEs of mutants are only 0.5 % higher than that of PO1f and 0.2 % lower than that of the biodiesel standard. Similarly, the heating values of FAMEs of mutants are only 0.5 % lower than those of PO1f and the biodiesel standard.

As for the temperature related properties, the FAMEs of mutants showed lower flash points at about 155 °C compared to 163 °C for PO1f, where those of *mfe*1Δ and biodiesel standard are close to 161 °C, and 155 °C, respectively (Table 7). Interestingly, the temperatures of the cold flow properties (CP, PP and CFPP) of biodiesels of mutants showed to be at least 10 °C lower than those of PO1f. Of all mutants, *mfe1*Δ showed to be associated with the lowest temperatures, at 1.11 °C (CP), −4.01 °C (PP) and −3.39 °C (CFPP). This entails that the biodiesel of *mfe1*Δ mutant should be associated with the best cold flow properties (Table 7). The *mfe1*Δ mutant showed to have close cold flow properties to that of the biodiesel standard, although the latter is associated with temperatures that are slightly lower for CP, PP and CFPP at 0.83, −4.29 and −3.67 °C, respectively.

The oxidation stability of biodiesel is a function of its unsaturated content. FAMEs originating from mutants have 10 % higher content of unsaturation than the PO1f (~74 % in mutants and ~64 % in PO1f), though 10 % lower than that in the biodiesel standard B100 (84.37 %) (Table 6). Therefore, FAMEs of mutants are expected to be associated with lower oxidation stability than that of PO1f, yet with a higher stability than that of biodiesel standard B100.

Overall, these results demonstrate the genetic and biochemical targets to be addressed when producing genetically engineered biodiesel (GEB) having optimized properties.

3.7. Predictions of emissions of biodiesels of constructed mutants

Currently, no precise mathematical model allows prediction of NO_X emissions. Nonetheless, nitric oxide (NO) emissions, one of the NO_X, was reported to inversely correlate with the content of saturated FAME as estimated by the straight-chain saturated factor (SCSF) at different engine loads (Navaneeth et al., 2021). It should be mentioned however that the reported NO emissions as a function of SCSF have low predictive accuracy with an error of about 23 % (Navaneeth et al., 2021). As mutant lipids have 40 % lower SCSF than that of PO1f, increased NO_X emissions are expected from mutant compared to PO1f biodiesels (Table 6). On the other hand, the FAME of mutants have 50 % higher SCSF than that of the biodiesel standard, B100, and thus is expected to have lower emissions of NO_X.

Overall, FAMEs of the mutants are distinguished for their higher degrees of unsaturation compared to that of the PO1f, which reflects predominantly on lesser CN and improved cold flow properties. Compared to the biodiesel standard, FAMEs of the mutants demonstrate overall better ignition quality and emission properties. Again, this work demonstrates the critical elements to be considered while producing genetically engineered biodiesel (GEB) having optimized properties via the genetic modifications of microbial lipids.

3.8. Compliance of mutants-derived biodiesels to theoretical optimum and to standard specifications

It was then verified to what extent the properties of FAMEs of the mutant strains, and most particularly the *mfe*1Δ, meet the international (ASTM) and European (EN) standard specifications of biodiesels, respectively ASTM D6751 (ASTM, 2023) and EN 14214 (EN, 2019).

Here, the FAMEs of the *mfe1*Δ mutant showed to conform to standard specification in terms of flash point, viscosity, cetane number and density (Tables 4 and 7). As for the temperature related properties, CP and CFPP, no specifications are available because this should be defined depending on the climate of the area where the biodiesel is meant to be used. Certainly, for cold climates like in Canada, biodiesel composition should be optimized to be operable at the lowest possible temperatures. This latter is also particularly important when knowing that the major limitation of biodiesel usage at 100 % blend (B100, i.e. unblended with petrodiesel) is their poor cold flow properties.

Although, the biodiesel of mutants did not exactly meet the theoretical optimum (17.36 C_X; 1.33 N_{DB}), the *mfe1*Δ mutant is closest to that and could be improved by further genetic engineering. Overall, the FAMEs of constructed mutants are distinguished by their higher unsaturated content than the parent PO1f strain, which reflects predominantly on slightly lower CN and improved cold flow properties though they are close to the properties of the biodiesel standard B100.

This is a proof of concept of the possibility of producing Genetically Engineered Biodiesel (GEB) with optimized properties derived from tailor feedstock oils designed by the genetic modifications of oleaginous yeast platforms.

3.9. Lipid profiling of other yeasts and prediction of their FAME properties

As to identify other sources of microbial oil potentially having natural optimal FAME composition, different oleaginous yeasts were

examined. The yeasts *Rhodotorula toruloides* Y-6987, *Starmerella bombicola* Y-5391, *Lipomyces starkeyi* Y-11561 and *Cutaneotrichosporon curvatus* YB-775 were grown in supplemented lipogenic media YNB glycerol:NH_4Cl (50:6 g/L) with yeast extract 1 g/L for 48 h as to support growth of all yeasts.

Analysis of respective transesterified lipid composition by GC-FID-MS, revealed interesting profiles, particularly with *S. bombicola* Y-5391. Fatty acid composition in *S. bombicola* Y-5391 is mainly consisting of oleic acid ($C_{18:1n-9}$) at 60 % of total lipid composition with lower amounts of palmitoleic ($C_{16:1n-7}$), palmitic ($C_{16:0}$) and stearic ($C_{18:0}$) acid at 10 % each (Table S2). On the other hand, the profiles *R. toruloides* Y-6987, *L. starkeyi* Y-11561 and *C. curvatus* YB-775 are closely similar to that of *Y. lipolytica* PO1f with similar amounts of palmitic ($C_{16:0}$) and linoleic ($C_{18:2n-6}$) (Table S2). However, all yeasts have an average chain length slightly higher than that of PO1f at about 17.5. With respect to unsaturation degree, *R. toruloides* Y-6987 and *S. bombicola* Y-5391 have lesser unsaturation (N_{DB} = ~0.7) than that of PO1f (Table 6), whereas *C. curvatus* YB-775 exhibit higher unsaturation degree (N_{DB} = ~0.9) (Table 6). The FAMEs of those yeasts were predicted to have cetane numbers as high as 62 and significantly higher viscosities (Table 7). In terms of temperature-related properties, most of these yeasts' FAMEs have equivalent or higher CP, PP and CFPP to those of PO1f, except for the FAMEs of *S. bombicola* Y-5391 whose respective CP, PP and CFPP at 7.56, 2.31 and 3.06 °C (Table 7). Based on those predictions, *S. bombicola* Y-5391 has a potential for the development of an optimal biodiesel that is operable in cold climates because of its cold flow properties and its enriched $C_{18:1}$ content.

This entails that optimal oil compositions could be screened for in alternative oleaginous yeasts to act as platforms for the production of a diversity of Genetically Engineered Biodiesel (GEB) encompassing a wide range of desired properties.

4. Conclusions

This study demonstrates that the genetic modification in *Y. lipolytica* for altering its lipid composition is a promising approach to generate tailored feedstock oils for the production of a new generation of biodiesel that we name genetically engineered designer biodiesel (GEB). Here, several simple and combined mutations led to the generation of different lipid profiles whose FAMEs is predicted to be associated with, amongst other, improved cold flow properties. Moreover, *in silico* optimisation of biodiesel composition led to the definition of potential optimal FAME composition consisting of an average chain length of 17.36 and degree of unsaturation of 1.33. This could guide different strategies for rational modifications and improvements of biodiesel composition to efficiently generate designer biodiesel with interesting properties and performances.

CRediT authorship contribution statement

Benjamin Ouellet: Methodology, Data curation, Validation, Formal Analysis, Investigation, Visualization, Writing – original draft. **A.M. Abdel-Mawgoud:** Conceptualization, Funding acquisition, Resources, Project administration, Supervision, Investigation, Validation, Formal Analysis, Writing – review & editing. All authors read and approved the manuscript.

Declaration of competing interest

The authors declare that they have no known competing financial interests or personal relationships that could have appeared to influence the work reported in this paper.

Data availability

All data generated or analyzed during this study are included in the supplementary material.

Acknowledgement

This work was funded by NSERC-Discovery Grant, Canada (RGPIN-2022-05307) and Fonds de recherche du Québec–Nature et technologies (FRQNT)-Établissement de la Relève Professorale, Quebec, Canada (Application no. 2022-NC-298442), to Professor Ahmad M. Abdel-Mawgoud. Mr. Benjamin Ouellet was a MSc student and was funded by Fonds de recherche du Québec - Nature et technologies (FRQNT)-MSc scholarship, Quebec, Canada.

Appendix A. Supplementary material

Supplementary data to this article can be found online at https://doi.org/10.1016/j.crbiot.2024.100189.

References

Abdel-Mawgoud, A.M., Markham, K.A., Palmer, C.M., Liu, N., Stephanopoulos, G., Alper, H.S., 2018. Metabolic engineering in the host Yarrowia lipolytica. Metab. Eng. 50, 192–208.

Abdel-Mawgoud, A.M., Stephanopoulos, G., 2020. Improving CRISPR/Cas9-mediated genome editing efficiency in *Yarrowia lipolytica* using direct tRNA-sgRNA fusions. Metab. Eng. 62, 106–115.

Anuchaya, D., Renuka, B., Dhanapati, D. 2016. Designer biodiesel: an optimization of fuel quality by blending multiple oils. In: Kumar, S., Khanal, S.K., Yadav, Y.K. (Eds.), Proceedings of the First International Conference on Recent Advances in Bioenergy Research, New Delhi. Springer India, New Delhi, pp. 131–148.

ASTM, 2023. ASTM D6751-23a: Specification for biodiesel fuel blend stock (B100) for middle distillate fuels. ASTM International, West Conshohocken, PA.

Beopoulos, A., Mrozova, Z., Thevenieau, F., Le Dall, M.-T., Hapala, I., Papanikolaou, S., Chardot, T., Nicaud, J.-M., 2008. Control of lipid accumulation in the yeast *Yarrowia lipolytica*. Appl. Environ. Microbiol. 74 (24), 7779–7789.

Blazeck, J., Hill, A., Liu, L., Knight, R., Miller, J., Pan, A., Otoupal, P., Alper, H.S., 2014. Harnessing *Yarrowia lipolytica* lipogenesis to create a platform for lipid and biofuel production. Nat. Commun. 5 (1), 3131.

Dulermo, T., Nicaud, J.M., 2011. Involvement of the G3P shuttle and beta-oxidation pathway in the control of TAG synthesis and lipid accumulation in *Yarrowia lipolytica*. Metab. Eng. 13 (5), 482–491.

Dunn, R.O., 2015. Cold flow properties of biodiesel: a guide to getting an accurate analysis. Biofuels 6 (1–2), 115–128.

EN, 2019. EN 14214: Liquid petroleum products - Fatty acid methyl esters (FAME) for use in diesel engines and heating applications - Requirement and test methods. European Committee for Standardization.

Gomez-Rodriguez, K.A., Chavarria-Hernandez, J.C., Martinez-Tapia, G.E., 2021. Estimation of cold flow properties of biodiesel from fatty acid composition. Energy Fuel 35 (2), 1442–1448.

Hoekman, S.K., Broch, A., Robbins, C., Ceniceros, E., Natarajan, M., 2012. Review of biodiesel composition, properties, and specifications. Renew. Sust. Energ. Rev. 16 (1), 143–169.

Joshi, R.M., Pegg, M.J., 2007. Flow properties of biodiesel fuel blends at low temperatures. Fuel 86 (1–2), 143–151.

Kinney, A.J., Clemente, T.E., 2005. Modifying soybean oil for enhanced performance in biodiesel blends. Fuel Process. Technol. 86 (10), 1137–1147.

Knothe, G., 2005. Dependence of biodiesel fuel properties on the structure of fatty acid alkyl esters. Fuel Process. Technol. 86 (10), 1059–1070.

Knothe, G., 2008. "Designer" biodiesel: Optimizing fatty ester composition to improve fuel properties. Energy Fuel 22 (2), 1358–1364.

Luo, Y.S., Nicaud, J.M., Van Veldhoven, P.P., Chardot, T., 2002. The acyl-CoA oxidases from the yeast *Yarrowia lipolytica*: characterization of Aox2p. Arch. Biochem. Biophys. 407 (1), 32–38.

Mlícková, K., Roux, E., Athenstaedt, K., d'Andrea, S., Daum, G., Chardot, T., Nicaud, J. M., 2004. Lipid accumulation, lipid body formation, and acyl coenzyme A oxidases of the yeast *Yarrowia lipolytica*. Appl. Environ. Microbiol. 70 (7), 3918–3924.

Moser, B.R., 2014. Impact of fatty ester composition on low temperature properties of biodiesel-petroleum diesel blends. Fuel 115, 500–506.

Nambou, K., Zhao, C., Wei, L.J., Chen, J., Imanaka, T., Hua, Q., 2014. Designing of a "cheap to run'' fermentation platform for an enhanced production of single cell oil from *Yarrowia lipolytica* DSM3286 as a potential feedstock for biodiesel. Bioresour. Technol. 173, 324–333.

Navaneeth, P.V., Suraj, C.K., Mehta, P.S., Anand, K., 2021. Predicting the effect of biodiesel composition on the performance and emission of a compression ignition engine using a phenomenological model. Fuel 293, 17.

Ng, T.K., Yu, A.Q., Ling, H., Juwono, N.K.P., Choi, W.J., Leong, S.S.J., Chang, M.W., 2020. Engineering *Yarrowia lipolytica* towards food waste bioremediation: Production of fatty acid ethyl esters from vegetable cooking oil. J. Biosci. Bioeng. 129 (1), 31–40.

Okoro, V., Azimov, U., Munoz, J., Hernandez, H.H., Phan, A.N., 2019. Microalgae cultivation and harvesting: growth performance and use of flocculants - a review. Renew. Sust. Energ. Rev. 115, 16.

Ouellet, B., Abdel-Mawgoud, A.M., 2023. Strong expression of Cas9 under a new 3'-truncated *TEF*1α promoter enhances CRISPR-Cas9-mediated genome editing in *Yarrowia lipolytica*. Curr. Res. Biotechnol., 100147

Ouellet, B., Morneau, Z., Abdel-Mawgoud, A.M., 2023. Nile red-based lipid fluorometry protocol and its use for statistical optimization of lipids in oleaginous yeasts. Appl. Microbiol. Biotechnol. 107 (23), 7313–7330.

Papanikolaou, S., Aggelis, G., 2011. Lipids of oleaginous yeasts. Part II: Technology and potential applications. Eur. J. Lipid Sci. Technol. 113 (8), 1052–1073.

Park, J.Y., Kim, D.K., Lee, J.P., Park, S.C., Kim, Y.J., Lee, J.S., 2008. Blending effects of biodiesels on oxidation stability and low temperature flow properties. Bioresour. Technol. 99 (5), 1196–1203.

Pinzi, S., Rounce, P., Herreros, J.M., Tsolakis, A., Dorado, M.P., 2013. The effect of biodiesel fatty acid composition on combustion and diesel engine exhaust emissions. Fuel 104, 170–182.

Qi, Y., Liu, H., Yu, J., Chen, X., Liu, L., 2017. Med15B regulates acid stress response and tolerance in *Candida glabrata* by altering membrane lipid composition. Appl. Environ. Microbiol. 83 (18), e01128–e10217.

Ramirez-Verduzco, L.F., Rodriguez-Rodriguez, J.E., Jaramillo-Jacob, A.D., 2012. Predicting cetane number, kinematic viscosity, density and higher heating value of biodiesel from its fatty acid methyl ester composition. Fuel 91 (1), 102–111.

Ratledge, C., Wynn, J.P., 2002. The biochemistry and molecular biology of lipid accumulation in oleaginous microorganisms. Adv. Appl. Microbiol. 51, 1–51.

Santos, S.M., Wolf-Maciel, M.R., Fregolente, L.V., 2023. Cold flow properties: Applying exploratory analyses and assessing predictive methods for biodiesel and diesel-biodiesel blends. Sustain. Energy Technol. Assess. 57, 19.

Sarin, A., Arora, R., Singh, N.P., Sarin, R., Malhotra, R.K., Sarin, S., 2010. Blends of biodiesels synthesized from non-edible and edible oils: effects on the cold filter plugging point. Energy Fuel 24 (3), 1996–2001.

Saxena, P., Jawale, S., Joshipura, M.H., 2013. A review on prediction of properties of biodiesel and blends of biodiesel. In: Chemical, Civil and Mechanical Engineering Tracks of 3rd Nirma University International Conference on Engineering (Nuicone2012), Vol. 51, pp. 395–402.

Schwartz, C., Shabbir-Hussain, M., Blenner, M., Wheeldon, I., 2016. Synthetic RNA polymerase III promoters facilitate high-efficiency CRISPR-Cas9-mediated genome editing in *Yarrowia lipolytica*. ACS Synth. Biol. 5 (4), 356–359.

Serrano, M., Oliveros, R., Sanchez, M., Moraschini, A., Martinez, M., Aracil, J., 2014. Influence of blending vegetable oil methyl esters on biodiesel fuel properties: Oxidative stability and cold flow properties. Energy 65, 109–115.

Singh, D., Sharma, D., Soni, S.L., Sharma, S., Sharma, P.K., Jhalani, A., 2020. A review on feedstocks, production processes, and yield for different generations of biodiesel. Fuel 262, 15.

Sorate, K.A., Bhale, P.V., 2015. Biodiesel properties and automotive system compatibility issues. Renew. Sust. Energ. Rev. 41, 777–798.

Su, Y.-C., Liu, Y.A., Diaz Tovar, C.A., Gani, R., 2011. Selection of prediction methods for thermophysical properties for process modeling and product design of biodiesel manufacturing. Ind. Eng. Chem. Res. 50 (11), 6809–6836.

Van Wychen, S., Ramirez, K., Laurens, L.M.L., 2016. Determination of Total Lipids as Fatty Acid Methyl Esters (FAME) by in situ Transesterification: Laboratory Analytical Procedure (LAP) (NREL/TP-5100-60958).

Vijayan, S.K., Naveena Victor, M., Sudharsanam, A., Chinnaraj, V.K., Nagarajan, V., 2018. Winterization studies of different vegetable oil biodiesel. Bioresource Technology Reports 1, 50–55.

Wahlen, B.D., Morgan, M.R., McCurdy, A.T., Willis, R.M., Morgan, M.D., Dye, D.J., Bugbee, B., Wood, B.D., Seefeldt, L.C., 2013. Biodiesel from microalgae, yeast, and bacteria: Engine performance and exhaust emissions. Energy Fuel 27 (1), 220–228.

Wang, J.P., Ledesma-Amaro, R., Wei, Y.J., Ji, B.Y., Ji, X.J., 2020. Metabolic engineering for increased lipid accumulation in *Yarrowia lipolytica*-a review. Bioresour. Technol. 313, 11.

Wu, F.J., Wang, J.X., Chen, W.M., Shuai, S.J., 2009. A study on emission performance of a diesel engine fueled with five typical methyl ester biodiesels. Atmos. Environ. 43 (7), 1481–1485.

Yuan, M.H., Chen, Y.H., Chen, J.H., Luo, Y.M., 2017. Dependence of cold filter plugging point on saturated fatty acid profile of biodiesel blends derived from different feedstocks. Fuel 195, 59–68.

Zhang, L., Loh, K.C., Kuroki, A., Dai, Y.J., Tong, Y.W., 2021. Microbial biodiesel production from industrial organic wastes by oleaginous microorganisms: current status and prospects. J. Hazard. Mater. 402, 18.

Zhao, C., Gu, D.Q., Nambou, K., Wei, L.J., Chen, J., Imanaka, T., Hua, Q., 2015. Metabolome analysis and pathway abundance profiling of *Yarrowia lipolytica* cultivated on different carbon sources. J. Biotechnol. 206, 42–51.